A&A 487, 1203–1208 (2008)
DOI: 10.1051/0004-6361:200809998

Astronomy & Astrophysics

Electron-impact excitation of Be-like Mg⋆

G. Del Zanna[1,2], I. Rozum[1], and N. R. Badnell[3]

[1] MSSL, University College London, Holmbury St., Mary, Dorking RH5 6NT, UK
e-mail: G.Del-Zanna@damtp.cam.ac.uk;GDelZanna@spd.aas.org
[2] DAMTP, Centre for Mathematical Sciences, Wilberforce road, Cambridge CB3 0WA, UK
[3] Department of Physics, University of Strathclyde, Glasgow G4 0NG, UK

Received 17 April 2008 / Accepted 13 June 2008

ABSTRACT

We present an *R*-matrix calculation of electron-impact excitation of Be-like Mg. The calculation is similar to that one presented for Be-like Fe by Chidichimo et al. (2005, A&A, 430, 331), and was done with the intermediate-coupling frame transformation method and including a total of 98 fine-structure levels, up to $n = 4$. We find significant differences with the widely used $n = 2$ excitation rates of Keenan et al. (1986, Phys. Scr., 34, 216), calculated by interpolating *R*-matrix calculations along the Be-like sequence. We present a list of the most important transitions and a few comparisons with SOHO SUMER and CDS/GIS spectra of the solar corona. We show that previous long-standing discrepancies between observed and predicted line intensities are now resolved. We also show how temperatures of the solar corona were significantly underestimated. For example, a coronal hole inter-plume temperature of 850 000 K found by Wilhelm et al. (1998, ApJ, 500, 1023) is now revised to 1 160 000 K.

Key words. atomic data – techniques: spectroscopic – Sun: corona

1. Introduction

It is well known that emission lines from Be-like ions provide many density and temperature diagnostics for astrophysical plasmas. In particular, the intensity ratios of the resonance vs. the intercombination transitions in the Be-like sequence is an excellent temperature diagnostic. The ratio between the 2s 2p $^1P_1$–2p^2 $^1D_2$ and the intercombination transition is also a good diagnostic, considering that the lines always fall close in wavelength. Indeed, this ratio has provided one of very few direct measurements of electron temperatures in the solar corona from SOHO (see, e.g. Wilhelm et al. 1998). This is also due to the fact that the averaged solar corona has a temperature of 1 MK, where Mg IX is most abundant under equilibrium conditions. Earlier examples of the usefulness of the above two ratios are given for example by Keenan et al. (1984b), where the Mg IX level populations of Keenan et al. (1984a) were used.

However, a large number of discrepancies between predicted and measured intensities for various ions along the sequence have now been reported. For example, Landi et al. (2001) and Landi et al. (2002) reported discrepancies based on SOHO/SUMER observations, while Del Zanna (1999) reported other discrepancies based on SOHO/CDS observations.

Previous calculations of electron impact excitation for this ion include the Distorted Wave (DW) collision strengths of Sampson et al. (1984), with a basic set of configurations up to $n = 3$, and more recently by Bhatia & Landi (2007) up to $n = 5$. K. Berrington and co-authors, in a number of papers presented electron excitation data for C III, O V, Ne VII and Si XI calculated using the *R*-matrix method and LS coupling for transitions among the $n = 2$ levels. The $n = 2$ effective collision strengths along the sequence were interpolated by Keenan et al. (1986) to provide rates for the other ions in the sequence. The Mg IX interpolated rates have been widely used in the literature, and have been included in the CHIANTI database (Dere et al. 1997). For example, the CHIANTI v.5 (Landi et al. 2006) Mg IX model includes the $n = 2$ interpolated collision strengths of Keenan et al. (1986), the DW data of Sampson et al. (1984) for the $n = 3$ transitions, and transition probabilities calculated with SUPERSTRUCTURE using a 15-configuration model of the ion.

In the present paper we present a complete set of electron impact excitations for $n = 2, 3, 4$ levels, calculated with the *R*-matrix approach, and investigate the reported discrepancies between observed and expected line intensities in the solar corona. This work is part of an on-going collaborative work (the APAP network[1]) to calculate and provide assessed atomic data for ions of astrophysical importance.

2. Calculation

For the electron scattering calculation, we have used the *R*-matrix method (Hummer et al. 1993; Berrington et al. 1995) in conjunction with the intermediate frame coupling transformation (ICFT) (see Badnell & Griffin 2001; Badnell et al. 2001). The calculations follow similar procedures for the Iron Project work on Be-like Fe published by Chidichimo et al. (2005). We used the AUTOSTRUCTURE code (Badnell 1997) to obtain the radial wavefunctions using radial scaling parameters to minimize the equally-weighted sum of all LS term energies in the Thomas-Fermi approximation. We included the mass-velocity, spin-orbit, and Darwin relativistic corrections. We adopted the

⋆ Full dataset of excitation and radiative data are only available in electronic form at the CDS via anonymous ftp to cdsarc.u-strasbg.fr (130.79.128.5) or via
http://cdsweb.u-strasbg.fr/cgi-bin/qcat?J/A+A/487/1203

[1] http://amdpp.phys.strath.ac.uk/UK_APAP

Table 1. Mg^{+8} target levels. Key: i: level index; Conf.: configuration; Level: level designation; E_{th}: theoretical level energy in Ry; E_{NIST} observed energy from the NIST database version 3 (with percentage difference between E_{th} and E_{NIST}).

i	Conf.	Level	E_{th}	E_{NIST} (%)	i	Conf.	Level	E_{th}	E_{NIST} (%)
1	$2s^2$	$^1S_0$	0.000	0.000	50	2s 4p	$^3P_1$	18.817	–
2	2s 2p	$^3P_0$	1.287	1.280 (0.55)	51	2s 4p	$^3P_2$	18.819	–
3	2s 2p	$^3P_1$	1.299	1.291 (0.65)	52	2s 4p	$^1P_1$	18.844	18.851 (–0.04)
4	2s 2p	$^3P_2$	1.323	1.313 (0.75)	53	2s 4d	$^3D_1$	18.944	18.954 (–0.05)
5	2s 2p	$^1P_1$	2.551	2.476 (2.96)	54	2s 4d	$^3D_2$	18.944	18.954 (–0.05)
6	$2p^2$	$^3P_0$	3.371	3.334 (1.10)	55	2s 4d	$^3D_3$	18.945	18.955 (–0.05)
7	$2p^2$	$^3P_1$	3.384	3.346 (1.12)	56	2s 4d	$^1D_2$	19.023	19.026 (–0.02)
8	$2p^2$	$^3P_2$	3.406	3.366 (1.20)	57	2s 4f	$^3F_2$	19.026	–
9	$2p^2$	$^1D_2$	3.778	3.692 (2.28)	58	2s 4f	$^3F_3$	19.026	–
10	$2p^2$	$^1S_0$	4.687	4.553 (2.86)	59	2s 4f	$^3F_4$	19.026	–
11	2s 3s	$^3S_1$	13.949	13.965 (–0.11)	60	2s 4f	$^1F_3$	19.049	–
12	2s 3s	$^1S_0$	14.187	14.198 (–0.08)	61	2p 4s	$^3P_0$	20.104	–
13	2s 3p	$^1P_1$	14.518	14.522 (–0.03)	62	2p 4s	$^3P_1$	20.112	–
14	2s 3p	$^3P_0$	14.539	14.557 (–0.13)	63	2p 4s	$^3P_2$	20.139	–
15	2s 3p	$^3P_1$	14.542	14.557 (–0.11)	64	2p 4s	$^1P_1$	20.196	–
16	2s 3p	$^3P_2$	14.547	14.557 (–0.07)	65	2p 4p	$^1P_1$	20.265	–
17	2s 3d	$^3D_1$	14.856	14.863 (–0.05)	66	2p 4p	$^3D_1$	20.288	–
18	2s 3d	$^3D_2$	14.857	14.864 (–0.05)	67	2p 4p	$^3D_2$	20.292	–
19	2s 3d	$^3D_3$	14.859	14.866 (–0.04)	68	2p 4p	$^3D_3$	20.314	20.319 (–0.02)
20	2s 3d	$^1D_2$	15.097	15.078 (0.13)	69	2p 4p	$^3S_1$	20.341	–
21	2p 3s	$^3P_0$	15.581	15.584 (–0.02)	70	2p 4p	$^3P_0$	20.347	–
22	2p 3s	$^3P_1$	15.592	15.594 (–0.01)	71	2p 4p	$^3P_1$	20.364	–
23	2p 3s	$^3P_2$	15.617	15.618 (–0.01)	72	2p 4p	$^3P_2$	20.368	20.370 (–0.01)
24	2p 3s	$^1P_1$	15.853	15.884 (–0.19)	73	2p 4d	$^3F_2$	20.396	–
25	2p 3p	$^1P_1$	15.928	15.930 (–0.02)	74	2p 4d	$^3F_3$	20.414	–
26	2p 3p	$^3D_1$	15.996	15.997 (–0.01)	75	2p 4d	$^1D_2$	20.419	20.423 (–0.02)
27	2p 3p	$^3D_2$	16.007	16.006 (0.01)	76	2p 4p	$^1D_2$	20.429	20.422 (0.03)
28	2p 3p	$^3D_3$	16.030	16.029 (0.00)	77	2p 4d	$^3F_4$	20.433	–
29	2p 3p	$^3S_1$	16.134	16.133 (0.01)	78	2p 4d	$^3D_1$	20.461	–
30	2p 3p	$^3P_0$	16.201	–	79	2p 4d	$^3D_2$	20.466	–
31	2p 3p	$^3P_1$	16.211	16.209 (0.01)	80	2p 4f	$^1F_3$	20.478	–
32	2p 3p	$^3P_2$	16.224	16.220 (0.02)	81	2p 4d	$^3D_3$	20.478	20.488 (–0.05)
33	2p 3d	$^3F_2$	16.276	–	82	2p 4f	$^3F_2$	20.481	–
34	2p 3d	$^3F_3$	16.294	–	83	2p 4f	$^3F_3$	20.481	–
35	2p 3d	$^1D_2$	16.305	16.308 (–0.02)	84	2p 4f	$^3F_4$	20.484	–
36	2p 3d	$^3F_4$	16.313	–	85	2p 4d	$^3P_2$	20.497	20.498 (–0.01)
37	2p 3p	$^1D_2$	16.395	16.365 (0.18)	86	2p 4d	$^3P_1$	20.503	20.503 (–0.00)
38	2p 3d	$^3D_1$	16.468	16.470 (–0.01)	87	2p 4d	$^3P_0$	20.506	–
39	2p 3d	$^3D_2$	16.472	16.474 (–0.01)	88	2p 4f	$^3G_3$	20.513	–
40	2p 3d	$^3D_3$	16.482	16.484 (–0.01)	89	2p 4f	$^3G_4$	20.517	–
41	2p 3d	$^3P_2$	16.545	16.542 (0.02)	90	2p 4f	$^3G_5$	20.530	–
42	2p 3d	$^3P_1$	16.552	16.551 (0.01)	91	2p 4f	$^3D_3$	20.541	–
43	2p 3d	$^3P_0$	16.556	16.555 (0.01)	92	2p 4f	$^1G_4$	20.544	–
44	2p 3p	$^1S_0$	16.693	–	93	2p 4f	$^3D_2$	20.546	–
45	2p 3d	$^1F_3$	16.760	16.719 (0.25)	94	2p 4f	$^3D_1$	20.555	–
46	2p 3d	$^1P_1$	16.807	16.782 (0.15)	95	2p 4p	$^1S_0$	20.561	–
47	2s 4s	$^3S_1$	18.592	–	96	2p 4f	$^1D_2$	20.566	–
48	2s 4s	$^1S_0$	18.684	–	97	2p 4d	$^1F_3$	20.589	20.563 (0.12)
49	2s 4p	$^3P_0$	18.816	–	98	2p 4d	$^1P_1$	20.600	20.579 (0.10)

same target as for Be-like Fe, namely 17 spectroscopic configurations up to $n = 4$ giving rise to 98 fine-structure levels and 4753 transitions. The theoretical target energies are shown in Table 1 along with the level identification and the observed energies taken from the National Institute of Standards and Technology (NIST) database[2] version 3. With a few exceptions in the lower levels, there is good agreement between the theoretical and observed energy levels. There is very little level mixing in the lower levels, so any departures from accurate level energies do not affect the collision strengths.

We calculated the full set of radiative transition probabilities A_{ji} (s^{-1}) amongst the 98 levels with AUTOSTRUCTURE. In the calculation of transition probabilities, we adopted experimental energies whenever available. In this paper, we did not attempt to match the collision rates with transition probabilities calculated with a large structure run, to avoid issues such as level matching. We note, however, that comparisons with previous literature have shown differences in transition probabilities within 15% (Bhatia & Landi 2007), and that, for the strongest lines, excellent agreement (within 5%) between our probabilities and the NIST compilation (cf. Table 2) can be found.

[2] http://physics.nist.gov

Table 2. List of the most prominent lines in Mg IX. Key: lower and upper level index; relative intensities (photons) Int = $N_j A_{ji}/N_e$, calculated at 10^8 cm^{-3}, and normalised to the intensity of the strongest transition; weighted absorption oscillator strength gf; Transition probability A_{ji} calculated with AUTOSTRUCTURE and as in the NIST v.3 database; transition description; observed wavelength λ_{ob} (Å).

$i-j$	Int	gf	A_{ji} (s^{-1})	A_{ji} (NIST)	Transition	λ_{ob}(Å)
1–5	1.0	0.31	5.1×10^9	5.15×10^9	$2s^2\ ^1S_0$–$2s\ 2p\ ^1P_1$	368.071
1–3	8.0×10^{-2}	2.1×10^{-5}	9.3×10^4	9.04×10^4	$2s^2\ ^1S_0$–$2s\ 2p\ ^3P_1$	706.060
4–8	2.7×10^{-2}	0.45	3.0×10^9	3.0×10^9	$2s\ 2p\ ^3P_2$–$2p^2\ ^3P_2$	443.973
4–7	1.1×10^{-2}	0.15	1.6×10^9	1.6×10^9	$2s\ 2p\ ^3P_2$–$2p^2\ ^3P_1$	448.294
3–8	9.5×10^{-3}	0.15	1.0×10^9	1.0×10^9	$2s\ 2p\ ^3P_1$–$2p^2\ ^3P_2$	439.176
2–7	8.8×10^{-3}	0.12	1.4×10^9	1.4×10^9	$2s\ 2p\ ^3P_0$–$2p^2\ ^3P_1$	441.199
5–9	1.4×10^{-2}	0.34	8.0×10^8	7.9×10^8	$2s\ 2p\ ^1P_1$–$2p^2\ ^1D_2$	749.552
1–4	1.1×10^{-2}	–	0.12	–	$2s^2\ ^1S_0$–$2s\ 2p\ ^3P_2$	694.006
3–7	6.5×10^{-3}	9.0×10^{-2}	1.0×10^9	1.0×10^9	$2s\ 2p\ ^3P_1$–$2p^2\ ^3P_1$	443.404
5–10	4.9×10^{-3}	0.22	7.8×10^9	7.6×10^9	$2s\ 2p\ ^1P_1$–$2p^2\ ^1S_0$	438.700
3–6	7.0×10^{-4}	0.12	4.0×10^9	4.0×10^9	$2s\ 2p\ ^3P_1$–$2p^2\ ^3P_0$	445.981

2.1. The collision strengths

The scattering calculation was performed using the intermediate-coupling frame transformation (ICFT) method. In the R-matrix inner region, exchange effects were included for $J = 0$–12, then extended to $J = 40$ using a non-exchange approximation. The contributions to infinite J were added using the Burgess sum rule (see Burgess 1974) for dipole transitions and a geometric series for the non-dipole transitions (see Badnell & Griffin 2001). In the outer region, an energy mesh of 1.28×10^{-3} Ry was used in the resonance region of the exchange calculation. A coarser mesh of 1.25 Ry was used beyond the resonance region of the exchange calculation and over the entire energy range of the non-exchange calculation up to an energy of 125 Ry. Collision strengths $\Omega(i-j)$ between all 4753 transitions among the 98 levels were calculated.

We extended the collision strengths beyond 125 Ry by using the method of scaling and extrapolating to the appropriate high-energy limits as described in Burgess & Tully (1992). The high-energy limits were calculated with AUTOSTRUCTURE for both optically-allowed (see Burgess et al. 1997) and forbidden transitions (see Chidichimo et al. 2003).

The collision strengths of the most important (populating) transitions have been visually inspected, together with the high-energy limits. Figure 1 shows a sample of collision strengths. Excellent agreement is found between our background values with the DW $\Omega(i-j)$ of Bhatia & Landi (2007), also shown in the plots. Bhatia & Landi (2007) performed a DW calculation for a set of 18 $n = 2, 3, 4, 5$ configurations giving rise to 92 fine structure levels. They found good agreement with the $n = 2, 3$ calculations of Sampson et al. (1984), with a few exceptions.

2.2. The effective collision strengths

We calculated the temperature-dependent effective collision strength $\Upsilon(i-j)$ by assuming a Maxwellian electron disribution:

$$\Upsilon(i-j) = \int_0^\infty \Omega(i-j)\exp(-E_j/kT)\,\mathrm{d}(E_j/kT)$$

where E_j is the final energy of the colliding electron (after excitation has occurred) and k is the Boltzmann constant. We performed the numerical integration by linearly interpolating the $\Omega(i,j)\exp(-E_j/kT)$ data points and extrapolating to the high-energy limit.

The effective collision strengths Υ were calculated in a wide temperature range (1.6×10^4–1.6×10^8 K) to cover all astrophysical applications. For collisionally-ionised plasmas, Mg^{+8} has peak abundance in equilibrium at 1×10^6 K as calculated by e.g. Mazzotta et al. (1998) and more recently by Bryans et al. (2006) using ionization and recombination rates in the low-density regime. High electron densities (say $>10^{10}$ cm^{-3}) can shift the peak ion abundance by only 20–30% (see Del Zanna & Mason 2003, for an example), however in photoionised plasmas the formation temperatures are much lower (Kallman & Bautista 2001).

Figure 2 shows effective collision strengths for a few important transitions. We found overall good agreement with the interpolated values of Keenan et al. (1986) for the dipole-allowed transitions, however significant differences are present for the forbidden transitions. These differences have an important impact on the whole level population for this ion.

3. Line intensities

The A_{ji} values, along with the collisional data, have been used to calculate, in equilibrium conditions, the fractional population $N_j(N_e, T_e)$ of the upper level j (relative to the total number density of the ion), as a function of electron temperature T_e and density N_e, by taking all excitations, de-excitations and cascading into account. The proton excitations within the $2s\ 2p\ ^3P$ levels, calculated by Ryans et al. (1998), have been included. We note, however, that they only slightly affect the overall level population for the ion. For example, at coronal conditions ($N_e = 10^8$ cm^{-3}, $T_e = 10^6$ K), the increase in population of the $2s\ 2p\ ^3P_1$ due to proton excitation from the $^3P_0$ is only 1/10 the increase due to electron excitation from the ground state. Table 2 lists the transitions with largest intensities, calculated at 1 MK and with a coronal density of 10^8 cm^{-3}.

The resonance line, observed at 368.07 Å, is one of the brightest spectral lines in the EUV. It is blended with various weaker transitions, which can become non-negligible for temperatures much higher than 1 MK. After the resonance line, the brightest lines are the intercombination $2s^2\ ^1S_0$–$2s\ 2p\ ^3P_1$ observed at 706.06 Å, and the $2s^2\ ^1S_0$–$2s\ 2p\ ^3P_2$ observed

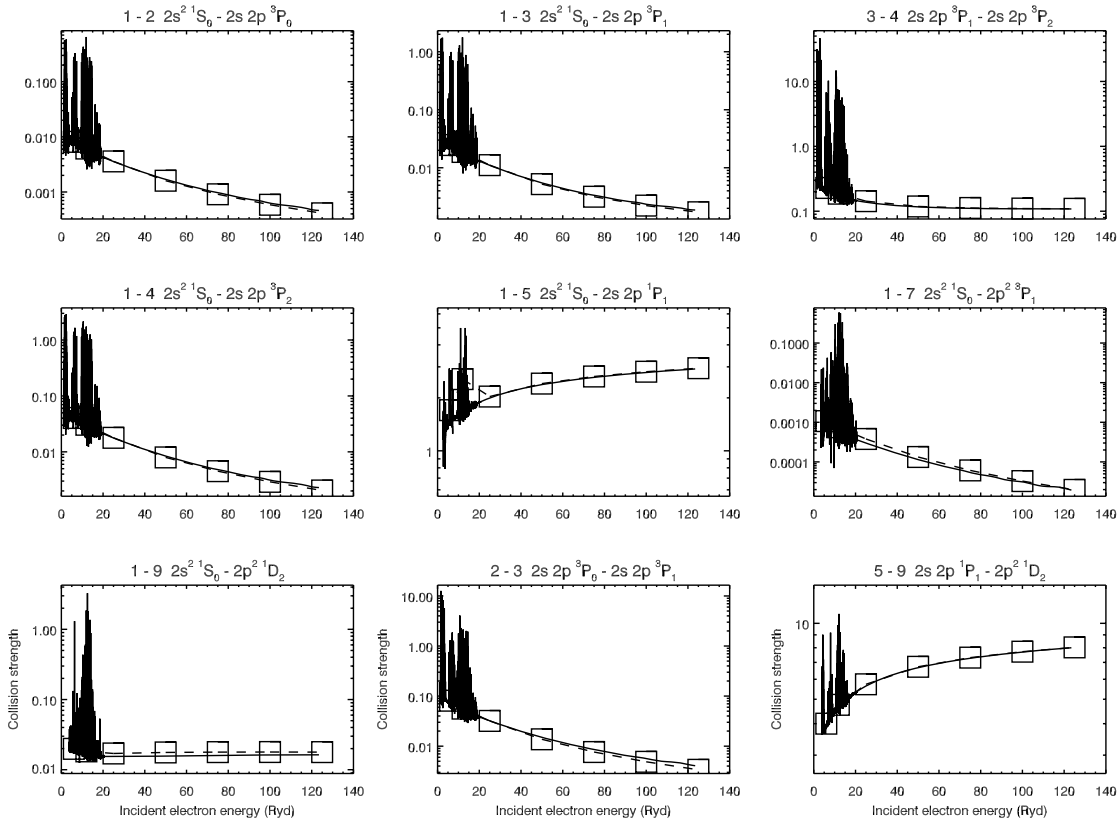

Fig. 1. $\log \Omega(i-j)$ as function of electron energy in rydbergs for a selection of transitions. Boxes indicate the DW values of Bhatia & Landi (2007).

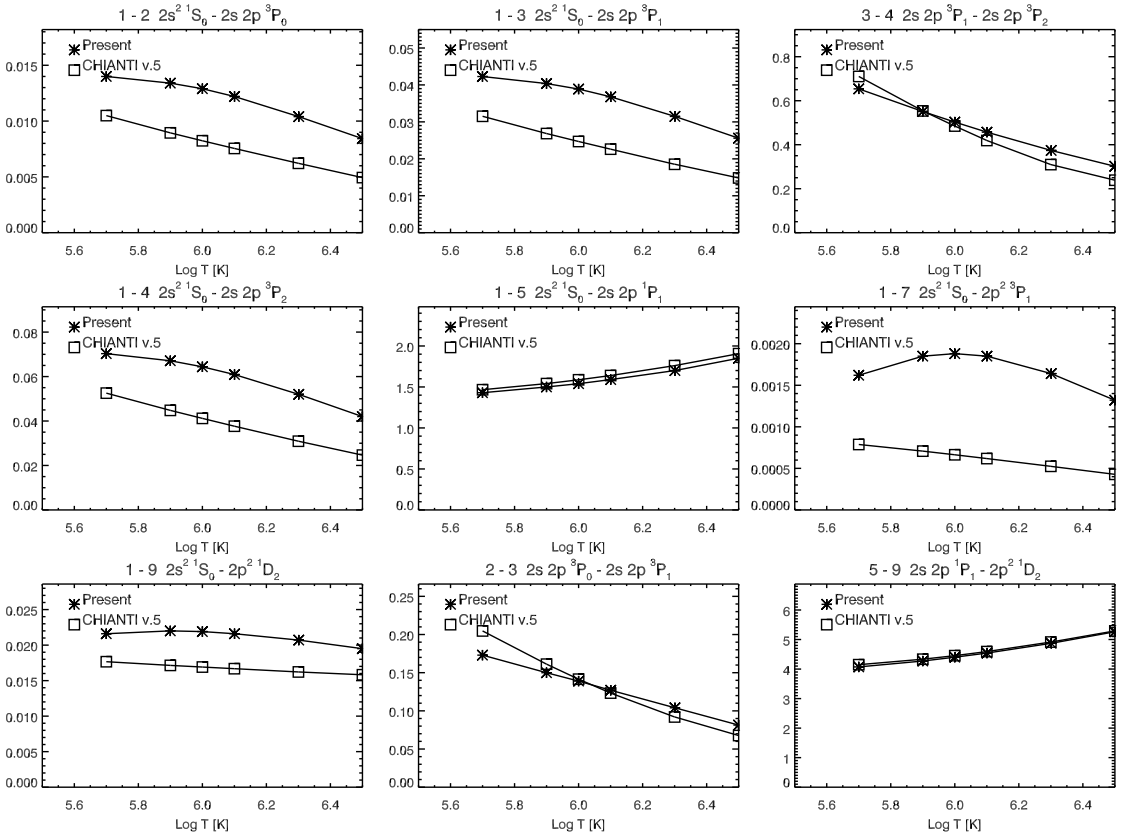

Fig. 2. Excitation rates as function of temperature for the same set of transitions displayed in Fig. 1. Boxes indicate the interpolated values of Keenan et al. (1986).

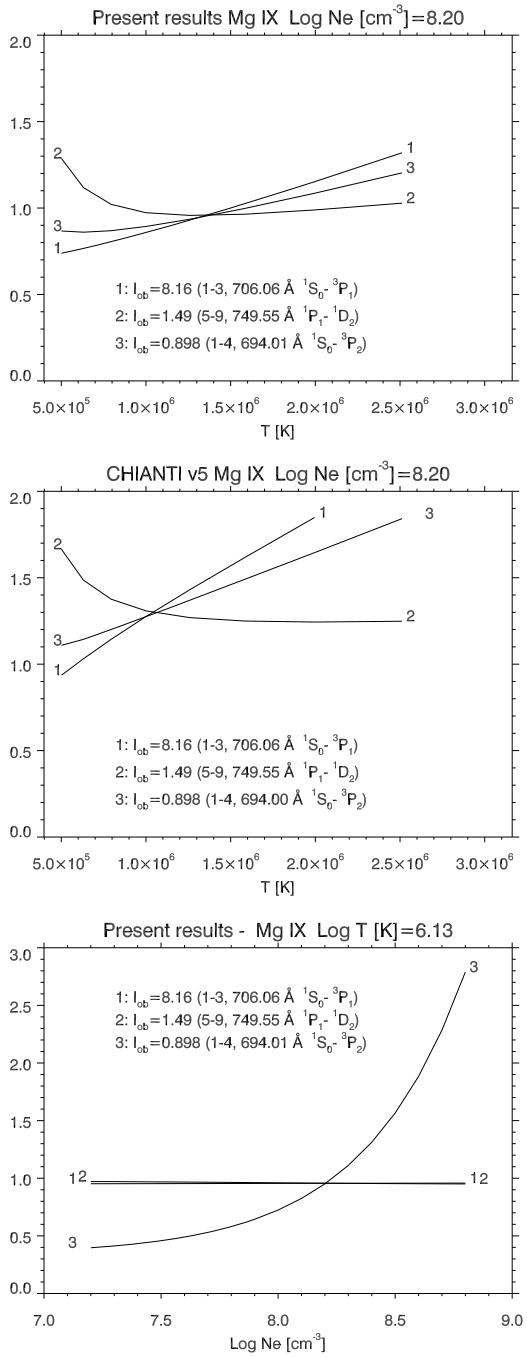

Fig. 3. Emissivity ratio curves of a SOHO/SUMER off-limb spectrum of the quiet solar corona (Feldman et al. 1999). For each line, we indicate: the observed intensities I_{ob}; the lower and upper level index corresponding to Table 1; the observed wavelength. *The upper and lower plots* were obtained with the present atomic data, while the middle one with CHIANTI v.5 (see text).

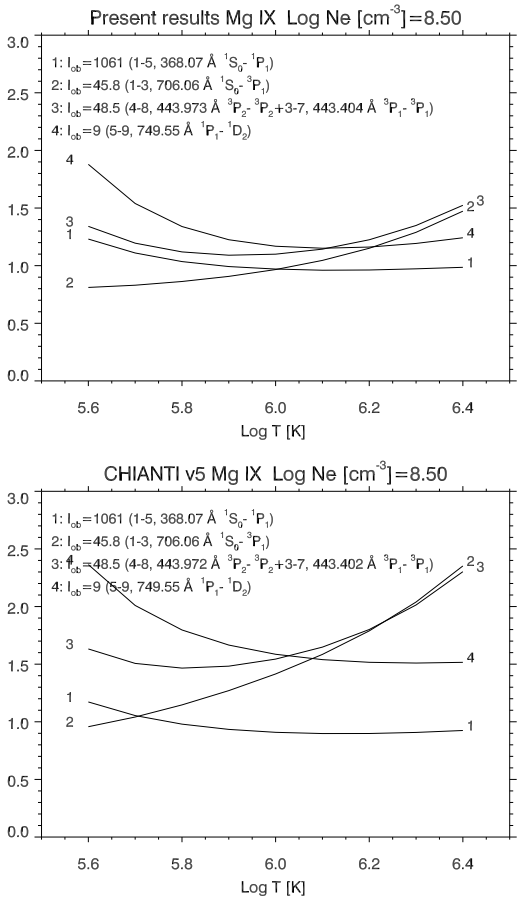

Fig. 4. Emissivity ratio curves from a SOHO/GIS off-limb spectrum of the quiet solar corona (Del Zanna 1999). The curves were calculated at $\log N = 8.5$, the electron density measured by line ratios of ions emitted at similar temperatures as Mg IX. *The upper plot* is with the present atomic data, while the lower one with the CHIANTI v.5 model.

at 694.0 Å. The lines from the 2s 2p–2p^2 transition array are weaker and mostly fall around 440 Å, with the exception of the important $^1P_1$–$^1D_2$ observed at 749.55 Å. Finally, many weaker $n = 3 \rightarrow n = 2$ transitions are observed in the X-rays.

We benchmark our calculations firstly against a set of SOHO/SUMER observations of the quiet off-limb solar corona (Feldman et al. 1999). The emitting plasma is well suited for the benchmark since it is approximately iso-density and iso-thermal. We adopt the measured intensities of Landi et al. (2002). The density was measured to be $\log N = 8.2$ (using line ratios) by Feldman et al. (1999). Figure 3 shows the emissivity ratio curves (Del Zanna et al. 2004):

$$F_{ji}(N_e, T_e) = C \quad \frac{I_{ob} N_e}{N_j(N_e, T_e)\, A_{ji}} \qquad (1)$$

calculated at a fixed density N_e as a function of temperature T_e (or vice-versa). I_{ob} is the observed intensity. The proportionality constant C is chosen for each dataset so that the emissivity ratios are close to unity. If agreement between observed and calculated intensities holds, the F_{ji} values for different spectral lines should overlap or cross, for an iso-density or iso-temperature plasma.

The crossing of the intercombination with the $^1P_1$–$^1D_2$ line in Fig. 3 indicates a temperature $T \simeq 1.35 \times 10^6$ K with the present atomic data, in excellent agreement with the independent measurement of Feldman et al. (1999), $1.35 \pm 0.05 \times 10^6$ K, obtained by assuming ionization equilibrium and comparing the abundances of different ions. The CHIANTI model, based on the interpolated values of Keenan et al. (1986), provides instead a lower temperature of $\simeq 1.0 \times 10^6$ K (note that Landi et al. 2002, quoted $T = 2.24 \times 10^6$ K, however this high value was possibly due to an error in the calculation, Landi, priv. comm.).

Wilhelm et al. (1998) measured with the SOHO SUMER instrument the ratios of the intercombination with the $^1P_1$–$^1D_2$ line as a function of the distance from the solar limb. They measured a photon ratio of 6.8 near the solar limb inside a

coronal hole, for both plume and inter-plume regions, where the density was approximately 10^8 cm^{-3}. They obtained T = 750 000 K. With the Keenan et al. (1986) excitation rates and the CHIANTI v.5 model, we obtain a close value of 720 000 K. With the present data, however, we obtain 830 000 K. In an inter-plume lane, the same authors measured a ratio of 6.0 at an approximate density of 10^7 cm^{-3} and at a radial distance of 0.3 $R_\odot$ from the limb. They obtained 850 000 K, while CHIANTI v.5 provides 810 000 K, and the present model 1 160 000 K (photo-excitation has been estimated assuming a black-body spectrum at 6000 K).

As already known from previous literature, the ratio of emissivities of these two lines is only slightly dependent from density, as shown in the lower plot of Fig. 3. This makes this ratio a good temperature diagnostic. The emissivity ratio of the $^1S_0$–$^3P_2$694.0 Å does instead depend on the density, as shown in the lower plot in Fig. 3, indicating an electron density of $\log N$ = 8.2, in excellent agreement with the values obtained from line ratios of lines from other ions.

The resonance and intercombination transitions provide an even better temperature diagnostic, considering their strength (the main limitation being blending of the resonance at $T >$ 1 MK). These lines are best observed when the resonance is recorded in second order (hence nearby the intercombination), as is the case for the SOHO Grazing Incidence Spectrometer (GIS), as described in Del Zanna (1999). Figure 4 shows the emissivity ratio curves from a SOHO/GIS off-limb spectrum of the quiet solar corona (Del Zanna 1999). The crossing of the intercombination with the resonance line $^1S_0$–$^1P_1$ indicates a temperature $\log T$ [K] $\simeq$ 6.0 with the present calculations, in agreement with the expected temperature. The strongest of the 2s 2p–2p^2 transitions that fall around 440 Å is a self-blend (at the GIS resolution), and indicates a density $\log N$ = 8.5. Close agreement, well within the estimated accuracy of the GIS radiometric calibration (30%, see Del Zanna et al. 2001) is found. The CHIANTI model indicates instead a much lower (and unrealistic) temperature $\log T$ [K] $\simeq$ 5.7, with a discrepancy of more than 50% between the resonance and the other lines.

Let us now briefly discuss how the differences between our calculation and CHIANTI v.5 in these line intensities (at about 1 MK) arise. The population of the 2s 2p $^1P_1$ is not significantly changed. The direct excitation from the ground state is about 5% lower, balanced by an increased cascade from the 2p^2 $^1D_2$ level, in turn due to a 25% increase in the direct excitation from the ground state. On the other hand, the population of the 2s 2p $^3P_1$ level is increased by 60%, due to a 60% increase in the direct excitation from the ground, and an increase due to cascading from the 2s 2p $^3P_2$ level. In turn, the population of the 2s 2p $^3P_2$ level is increased by 50% because of the increase in the direct excitation from the ground state (see Fig. 1).

4. Conclusions

We have presented a complete R-matrix calculation of electron-impact excitation of Be-like Mg up to n = 4, and compared our predicted line intensities with particularly well-suited SOHO SUMER and CDS/GIS observations of nearly iso-density and iso-thermal solar coronal plasma. We have found excellent agreement, which gives us confidence in the reliability of the present atomic data. Further work is in progress, to assess the reliability of available excitation data along this important isoelectronic sequence.

The previous long-standing discrepancies in the temperatures measured with Mg IX are now resolved. Previously, coronal temperatures have been underestimated. In particular, we have revised some coronal hole temperatures found by Wilhelm et al. (1998). These types of measurements are very important, considering that almost all temperature measurements found in the literature are not direct, and often obtained by assuming ionization equilibrium.

We have shown some of the excellent diagnostics available with Mg IX lines, however we note that others are present when considering the (weaker) n = 3, 4 lines. We strongly suggest that future solar spectrometers observe the 368.07 Å resonance line (in second order), together with the intercombination 706.06 Å, the 694.01, and 749.55 Å lines, which provide excellent direct measurements of both the electron density and temperature of 1 MK plasmas.

Acknowledgements. Support from the UK STFC (G.D.Z.: Advanced Fellowship; G.D.Z., N.R.B.: APAP network) is acknowledged. We thank the anonymous referee for careful reading of the manuscript.

References

Badnell, N. R. 1997, J. Phys. B Atom. Mol. Phys., 30, 1
Badnell, N. R., & Griffin, D. C. 2001, J. Phys. B Atom. Mol. Phys., 34, 681
Badnell, N. R., Griffin, D. C., & Mitnik, D. M. 2001, J. Phys. B Atom. Mol. Phys., 34, 5071
Berrington, K. A., Eissner, W. B., & Norrington, P. H. 1995, Comp. Phys. Comm., 92, 290
Bhatia, A. K., & Landi, E. 2007, Atom. Data Nucl. Data Tables, 93, 742
Bryans, P., Badnell, N. R., Gorczyca, T. W., et al. 2006, ApJS, 167, 343
Burgess, A. 1974, J. Phys. B Atom. Mol. Phys., 7, L364
Burgess, A., & Tully, J. A. 1992, A&A, 254, 436
Burgess, A., Chidichimo, M. C., & Tully, J. A. 1997, J. Phys. B Atom. Mol. Phys., 30, 33
Chidichimo, M. C., Badnell, N. R., & Tully, J. A. 2003, A&A, 401, 1177
Chidichimo, M. C., Del Zanna, G., Mason, H. E., et al. 2005, A&A, 430, 331
Del Zanna, G. 1999, Ph.D. Thesis, Univ. Central Lancashire, UK
Del Zanna, G., & Mason, H. E. 2003, A&A, 406, 1089
Del Zanna, G., Bromage, B. J. I., Landi, E., & Landini, M. 2001, A&A, 379, 708
Del Zanna, G., Berrington, K. A., & Mason, H. E. 2004, A&A, 422, 731
Dere, K. P., Landi, E., Mason, H. E., Monsignori Fossi, B. C., & Young, P. R. 1997, A&AS, 125, 149
Feldman, U., Doschek, G. A., Schühle, U., & Wilhelm, K. 1999, ApJ, 518, 500
Hummer, D. G., Berrington, K. A., Eissner, W., et al. 1993, A&A, 279, 298
Kallman, T., & Bautista, M. 2001, ApJS, 133, 221
Keenan, F. P., Berrington, K. A., Burke, P. G., Kingston, A. E., & Dufton, P. L. 1984a, MNRAS, 207, 459
Keenan, F. P., Kingston, A. E., Dufton, P. L., Doyle, J. G., & Widing, K. G. 1984b, Sol. Phys., 94, 91
Keenan, F. P., Berrington, K. A., Burke, P. G., Dufton, P. L., & Kingston, A. E. 1986, Phys. Scr., 34, 216
Landi, E., Doron, R., Feldman, U., & Doschek, G. A. 2001, ApJ, 556, 912
Landi, E., Feldman, U., & Dere, K. P. 2002, ApJS, 139, 281
Landi, E., Del Zanna, G., Young, P. R., et al. 2006, ApJS, 162, 261
Mazzotta, P., Mazzitelli, G., Colafrancesco, S., & Vittorio, N. 1998, A&AS, 133, 403
Ryans, R. S. I., Foster-Woods, V. J., Copeland, F., et al. 1998, Atom. Data Nucl. Data Tables, 70, 179
Sampson, D. H., Goett, S. J., & Clark, R. E. H. 1984, Atom. Data Nucl. Data Tables, 30, 125
Wilhelm, K., Marsch, E., Dwivedi, B. N., et al. 1998, ApJ, 500, 1023